J. Plasma Phys. (2026), *vol*. 92, E91 © The Author(s), 2026. Published by Cambridge University Press.
This is an Open Access article, distributed under the terms of the Creative Commons Attribution licence (https://creativecommons.org/licenses/by/4.0/), which permits unrestricted re-use, distribution and reproduction, provided the original article is properly cited. doi:10.1017/S0022377826101913

Status of the GDT experiment

Peter Bagryansky, Elena Soldatkina, Andrey Meyster, Vadim Prikhodko, Alexander Solomakhin, Vladimir Maximov, Alexander Khilchenko, Yury Kovalenko, Evgeniy Shmigelsky, Olga Korobeynikova, Evgeny Kolesnikov, Vitaly Korzh, Egor Pinzhenin, Ekaterina Puryga and Peter Zubarev

Budker Institute of Nuclear Physics, Lavrentiev Ave. 11, Novosibirsk, Russia

Corresponding author: Elena Soldatkina, e.i.soldatkina@inp.nsk.su

(Received 28 February 2026 UTC; revision received 28 February 2026 UTC; accepted 25 May 2026 UTC)

The Gas Dynamic Trap (GDT) facility at the Budker Institute of Nuclear Physics continues experimental studies in support of the Gas-Dynamic Multiple-Mirror Trap (GDMT) project – a prospective neutron source and thermonuclear reactor concept based on open-ended magnetic confinement. During the 2024–2025 upgrade campaign, key engineering systems and diagnostic suites were substantially modernised to address critical physics and technology challenges for the GDMT development. Three key research and development directions were pursued. First, a conductive wall stabilisation system was designed to suppress magnetohydrodynamic (MHD) instabilities at high plasma beta. Second, a new second-harmonic X-mode electron cyclotron resonance heating (ECRH) system operating at 54.5 GHz with 0.8 MW power was commissioned. Preliminary experiments demonstrated increased electron temperature compared with non-ECRH heated plasmas. Third, proof-of-principle experiments on bulk plasma fuelling using a Marshall gun injector were successfully performed, supporting further development towards a high-repetition-rate injector. These results provide essential experimental validation and technological groundwork for the GDMT project, demonstrating progress towards high-beta plasma operation, efficient heating schemes and particle balance control in open magnetic traps.

Key words: plasma confinement, plasma diagnostics, plasma heating

1. Introduction

The Gas Dynamic Trap (GDT) (Ivanov & Prikhodko 2013) is an experimental facility designed to test key technologies for confining hot plasma in open-ended magnetic traps with a linear axisymmetric configuration. The GDT research programme primarily aims to validate the design of the Gas-Dynamic Multiple-mirror Trap (GDMT) project (Skovorodin *et al.* 2023), currently under development at the Budker Institute of Nuclear Physics (BINP) in collaboration with several domestic and international organisations.

https://doi.org/10.1017/S0022377826101913 Published online by Cambridge University Press

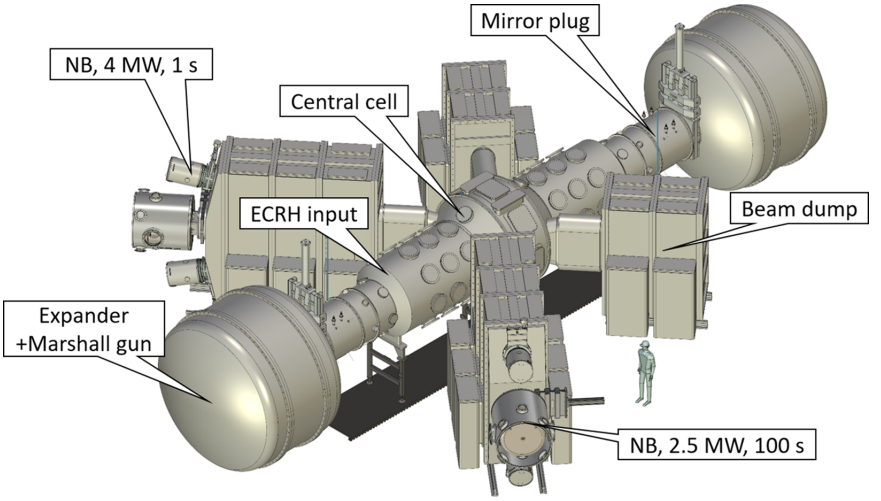


FIGURE 1. 3-D model of the first stage of the GDMT facility.

Over the past two years, the GDT diagnostic suite has undergone substantial upgrades, including Thomson scattering system, plasma energy balance diagnostics, diagnostics for thermonuclear reaction products and other advanced instrumentation (Soldatkina *et al.* 2025). These enhancements have significantly improved the accuracy of energy balance analysis during neutral beam injection heating. In particular, at least 85 % of the neutral beam power captured by the plasma has been successfully accounted for across various loss channels (Soldatkina *et al.* 2024). A series of experiments has been conducted to investigate the suppression of MHD instabilities through the interaction of high-beta plasma with surrounding conductive structures.

Experiments involving the injection of high-pressure plasma jets into the GDT have been performed to develop particle balance control technology for the GDT and future reactor-scale installations based on this concept. This injection method has proven effective both for generating the initial plasma required for neutral beam capture and for controlling plasma density during the main discharge phase. Additionally, electron cyclotron resonance heating (ECRH) experiments at the second harmonic have been carried out using a 54.5 GHz gyrotron with a power of up to 0.8 MW to provide supplementary heating of the electron component.

2. Main objectives of the experiment at the GDT facility

As noted in the introduction, the current GDT research programme aims to validate the design of the GDMT, whose technical design is under development.

In contrast to the earlier project version described in detail by Skovorodin *et al.* (2023), the new design features a magnetic system based entirely on superconducting coils. During the first phase of technical design, the central section of the magnetic trap – including expander sections and plasma heating systems – will be constructed. Figure 1 presents a three-dimensional (3-D) model of the first-stage GDMT facility.

The main parameters of the first stage of the GDMT facility are presented in table 1.

https://doi.org/10.1017/S0022377826101913 Published online by Cambridge University Press

Parameter	Value
Distance between mirrors	10 m
Plasma radius	15–30 cm
Magnetic field	
Central plane	0–1.5 T
Mirrors	20 T
NB injection (H_0)	
Total power	20 MW
Operation time	1 s
Total power	5 MW
Operation time	100 s
Energy of atoms	40 keV
Auxiliary ECRH	
Frequency	170 GHz
Total power	2 MW
Operation time	10 s

TABLE 1. Basic parameters of the first stage of the GDMT facility.

During the second development phase, multi-mirror (Budker, Mirnov & Ryutov 1971; Postupaev *et al.* 2017) or helical (Beklemishev 2013; Sudnikov *et al.* 2024) sections will be added to mitigate longitudinal particle and energy losses. The facility under design will establish a physical basis for thermonuclear applications, including a neutron source and a prospective thermonuclear reactor based on an open-ended magnetic trap with a linear axisymmetric configuration.

Calculations presented by Moyzykh *et al.* (2026) demonstrate that implementing the diamagnetic confinement regime with $\beta \to 1$ (Beklemishev 2016) in the central section, combined with effective suppression of axial losses by multi-mirror or helical sections, enables the development of deuterium–tritium (D–T) and even deuterium–deuterium (D–D) fusion reactors based on the GDMT concept operating under ignition conditions.

3. GDT facility

Figure 2 shows the GDT facility with its key components and primary diagnostic systems, which are described in detail by Soldatkina *et al.* (2025). Table 2 lists the main engineering parameters of the GDT device.

Previous experiments at the GDT facility have yielded the following key results in the physics of open-ended magnetic traps.

(i) A method for suppressing losses caused by MHD instabilities has been developed and a plasma beta of $\beta \geqslant 0.5$ has been achieved in an axisymmetric magnetic field configuration (Simonen *et al.* 2010).

(ii) Processes governing axial thermal transport have been investigated in detail. A technique to overcome classical Spitzer thermal conductivity has been developed and electron heating up to 1 keV has been demonstrated (Bagryansky *et al.* 2015; Soldatkina *et al.* 2020).

(iii) Approaches to mitigate the effects of kinetic instabilities have been identified Zaytsev *et al.* (2014).

https://doi.org/10.1017/S0022377826101913 Published online by Cambridge University Press

Parameter	Value
Distance between mirrors	7 m
Magnetic field	
Central plane	0.35 T
Mirrors	12 T
Mirror ratio	35
NB injection (D_0)	
Total power	5 MW
Operation time	5 ms
Energy of atoms	25 keV

TABLE 2. Main parameters of the GDT facility.

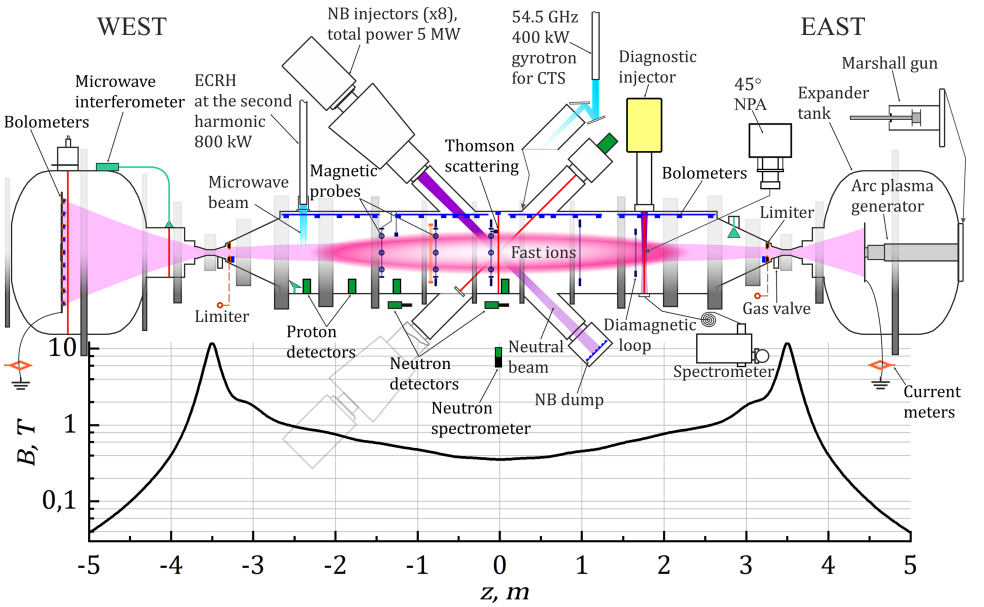


FIGURE 2. Scheme of the GDT facility with its key elements and basic diagnostics.

The current GDT experimental programme focuses on the following key tasks, essential for validating the GDMT project:

(i) development of MHD stabilisation techniques for high-beta plasma ($\beta \to 1$), including the use of a conductive wall and active feedback systems;
(ii) electron cyclotron resonance heating (ECRH) and generation of the initial plasma;
(iii) investigation of radial transport processes;
(iv) warm plasma fuelling.

https://doi.org/10.1017/S0022377826101913 Published online by Cambridge University Press

4. Upgrades to key GDT diagnostic systems

During the 2024–2025 upgrade campaign, several critical engineering systems and core diagnostic suites of the GDT facility were modernised.

(i) The vacuum system was converted to oil-free pumping technology.
(ii) The reliability of the magnetic mirror coils was enhanced.
(iii) A new second-harmonic X-mode electron cyclotron resonance heating system was developed.
(iv) Neutral beam power supply systems were redesigned for improved performance.
(v) The Thomson scattering diagnostic was upgraded to enhance spatial and temporal resolution.
(vi) A bolometer array was installed to measure charge-exchange losses in the central cell.
(vii) Diagnostics for fusion reaction products were expanded and modernised.
(viii) A Mirnov coil array was implemented for MHD instability monitoring.

4.1. *Upgrade of Thomson scattering diagnostics*

As a result of the upgrade, the Thomson scattering diagnostic system now enables time-resolved measurements of radial profiles of electron temperature and density. Its key components include:

(i) a Nd:YAG laser (wavelength 1064 nm) delivering a single pulse with 1.5 J energy;
(ii) a Beamtech SGR-30 PBLS laser operating at the same wavelength, providing 10 pulses per plasma shot with 3 J energy per pulse;
(iii) digital spectrometers based on bandpass interference filters for processing the scattered light signals (Lizunov *et al.* 2019).

A dedicated calibration procedure employing Raman scattering in molecular gases is performed to ensure accurate determination of the absolute electron density. The diagnostic system enables measurements of electron temperature in the range of 20 eV to 3 keV with an accuracy of 3 %. The arrangement of diagnostic components near the GDT vacuum vessel is shown schematically in figure 3.

Figure 4 presents an example of the time evolution of radial electron density and temperature profiles in standard GDT operation mode measured with the upgraded Thomson scattering diagnostic.

4.2. *Upgrade of fusion product diagnostics at GDT*

Experiments at the GDT facility are primarily carried out with deuterium plasma. The deuterium–deuterium (D–D) fusion reaction proceeds via two branches of approximately equal probability:

$$D + D \xrightarrow{50\%} {}^{3}He\ (0.82\ \mathrm{MeV}) + n\ (2.45\ \mathrm{MeV}), \tag{4.1}$$

$$D + D \xrightarrow{50\%} T\ (1.01\ \mathrm{MeV}) + p\ (3.02\ \mathrm{MeV}). \tag{4.2}$$

The fusion product diagnostics at GDT focus exclusively on detecting neutrons and protons. The spatial distribution of proton emission regions is measured using ultra-thin dead-layer silicon semiconductor detectors installed near the first wall inside the vacuum vessel. The GDT magnetic field is relatively weak; consequently,

https://doi.org/10.1017/S0022377826101913 Published online by Cambridge University Press

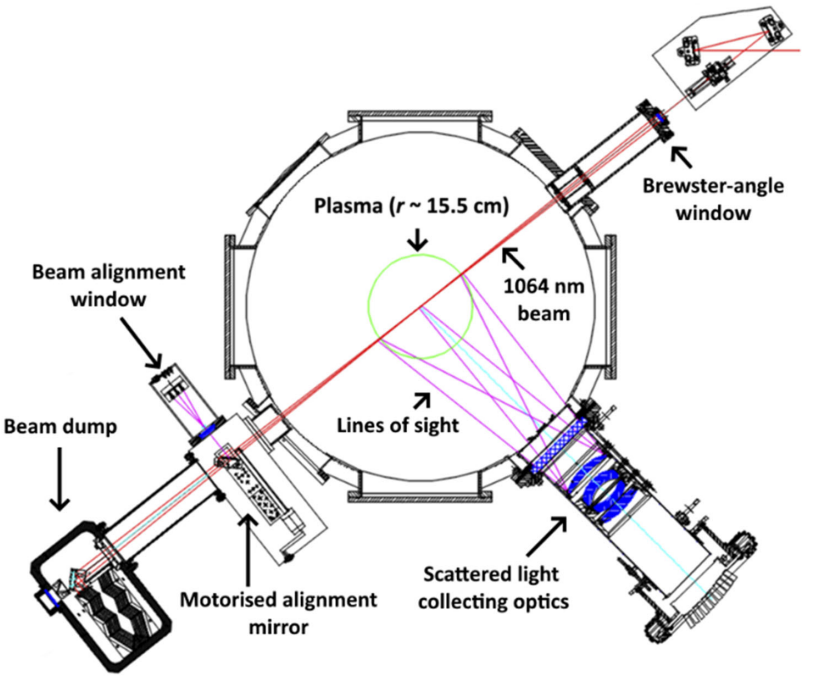


FIGURE 3. Arrangement of Thomson scattering diagnostic elements near the vacuum vessel of GDT device.

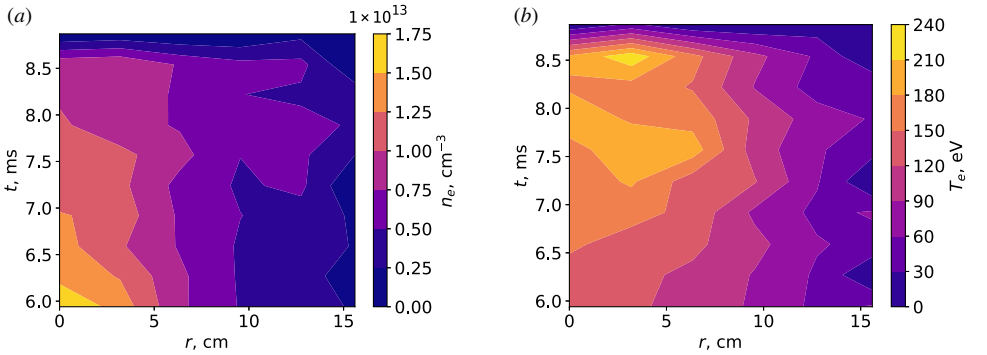


FIGURE 4. Examples of temporal profiles of (*a*) radial electron density and (*b*) temperature profiles measured with the upgraded Thomson scattering diagnostic system in one of the discharges.

the gyroradii of 3.02 MeV protons from D–D fusion exceed the vessel radius. This allows localisation of the proton emission region with a spatial resolution of $20 \times 20\,\mathrm{cm}^2$ using dedicated collimators (Pinzhenin & Maximov 2024).

Figure 5 shows an example of axial proton yield profiles measured before and after the onset of the Alfvén ion cyclotron (AIC) instability. The coordinate $z \approx 170$ cm corresponds to the turning point of hot ions with a pitch angle of 45°, matching the injection angle of the neutral beams. For comparison, results from the DOL

https://doi.org/10.1017/S0022377826101913 Published online by Cambridge University Press

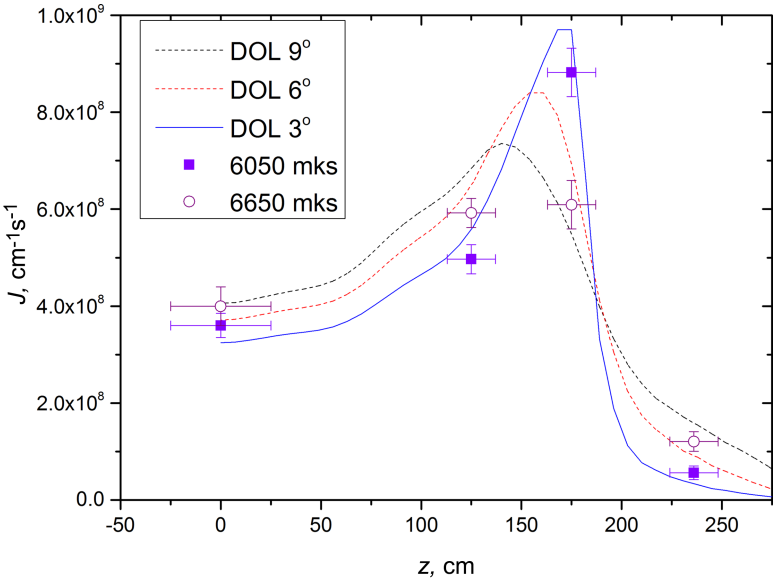


FIGURE 5. Axial proton yield profile measured before (6050 μs) and after (6650 μs) the onset of the Alfvén ion cyclotron (AIC) instability.

kinetic code (Yurov, Prikhodko & Tsidulko 2016) are presented for three values of the angular spread of the hot ion distribution function. An angular spread of 3° approximately corresponds to the intrinsic divergence of the neutral beams. The data in figure 5 demonstrate that AIC instability development leads to a moderate increase in the angular spread of hot ions, but does not cause significant scattering into the loss cone, confirming earlier conclusions reported by Zaytsev *et al.* (2014).

Neutron flux measurements are performed using organic scintillation detectors. This diagnostic system has been retained without major modifications during the recent upgrade campaign.

4.3. *Upgrade of energy balance diagnostics*

A key parameter of a prospective fusion reactor based on an open magnetic trap is its energy efficiency; therefore, studying possible energy loss channels from the system is critically important for validating the design of such a reactor. To establish the energy balance within the trap, it is necessary to measure the amounts of energy supplied to the plasma and lost from it through various channels. The considered potential energy loss channels include: longitudinal losses to the plasma collector located beyond the trap's mirror, losses to radial limiters that confine the plasma size and have direct contact with it, as well as losses due to charge exchange of plasma ions with residual gas. Research on energy loss channels is currently underway at the GDT, where a corresponding suite of diagnostics is being developed by Soldatkina *et al.* (2024).

In 2025, the system of pyroelectric bolometers measuring energy losses to the wall of the GDT central chamber was expanded with additional sensors. Eleven new detectors, equipped with shutters to protect against titanium deposition, were installed on the wall of the 'western' half of the vacuum chamber. Additionally, one more detector was installed in the 'eastern' half near the output ports of the neutral

https://doi.org/10.1017/S0022377826101913 Published online by Cambridge University Press

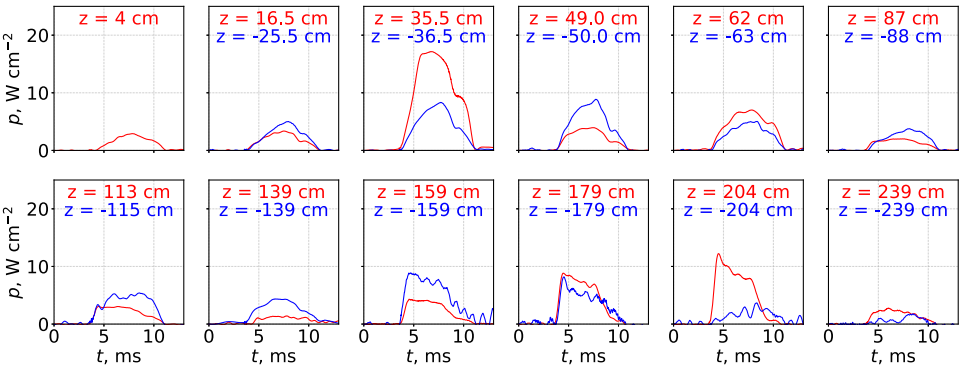


FIGURE 6. Example temporal dependencies of power losses to the vacuum chamber wall measured by the array of pyroelectric bolometers. Red colouring corresponds to the probes in the eastern half of the trap and blue to the western half.

beam injectors, as an elevated level of charge-exchange losses is expected in this region due to plasma interaction with an active target – specifically, the atoms of the injected beams.

All sensors are equipped with a galvanically isolated battery-powered supply system, activated by a light pulse from the facility's control system. Additionally, the data acquisition system for all sensors has been upgraded to extend the measurable signal range up to 66 W cm^{-2}.

The upgraded pyrobolometer system, which previously allowed measurements in only one half of the central chamber, now covers the entire length of the GDT. Consequently, it becomes possible to measure energy losses from the plasma caused by charge exchange of ions with residual neutral gas, as well as losses due to electromagnetic radiation emitted from the plasma. The system enables the study of both temporal and spatial dependencies of power losses through these channels. Figure 6 shows a charge-exchange loss distribution to the vacuum chamber wall that is characteristic of GDT under a standard magnetic configuration: the highest power fluxes should be observed near the turning points of fast ions ($z = \pm 190$ cm from the facility centre). However, the turning points have a certain width along the facility axis, which is why noticeable signals are also observed on adjacent sensors. Furthermore, the magnitude of charge-exchange losses strongly depends on the gas puffing scenario. In the example presented, gas was puffed from the eastern side of the facility, thus causing a high power density of charge-exchange losses to be observed on the $z = 204$ cm bolometer, located near the eastern turning point. Additionally, the high level of power flux at $z = 35$ cm is associated with the sensor's location near the output port of the injected neutral beams and is presumably determined by a high level of charge exchange of fast ions in this region.

Signals from individual sensors are used to calculate the total power losses to the vacuum chamber wall. For this purpose, the signal from each bolometer is multiplied by an area corresponding to the lateral surface of a cylinder with a radius of 45 cm (the distance from the facility axis to the sensors) and a height equal to the distance between the midpoints of the intervals to two adjacent sensors. Summing these values yields the instantaneous power losses to the facility wall; an example of such power calculations for one of the discharges is shown in figure 7.

https://doi.org/10.1017/S0022377826101913 Published online by Cambridge University Press

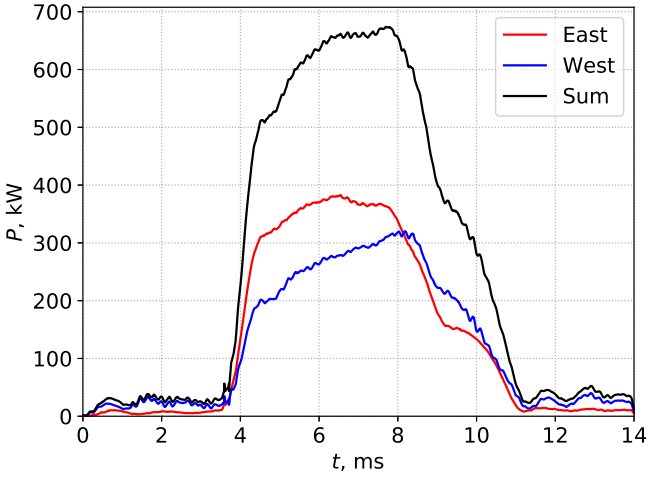


FIGURE 7. Example of total measured power losses to the central chamber walls of the GDT during a discharge measured by the array of pyroelectric bolometers.

5. MHD plasma stabilisation using a conductive wall

To mitigate transverse transport associated with MHD instabilities, the vortex confinement method (Beklemishev *et al.* 2010) is currently employed at GDT. This technique requires direct electrical contact between the plasma and absorber electrodes. However, if axial losses are reduced below a certain threshold, this electrical contact will be disrupted.

A potential solution involves a two-stage approach:

(i) transition to a high-beta regime using vortex confinement;
(ii) suppression of MHD-driven losses through the interaction of plasma diamagnetic currents with image currents induced in surrounding conductive structures.

MHD stabilisation by a conducting wall has been extensively investigated over recent decades (see, for example, Kaiser & Pearlstein 1985; Berk, Wong & Tsang 1987) and in more recent studies (Zeng & Kotelnikov 2024; Kotelnikov 2025). Recent analysis by Kotelnikov (2025) predicts the effectiveness of this stabilisation method for $\beta \geqslant 0.8$, provided that the conducting wall configuration surrounding the plasma is optimised.

One of the key parameters of a conductive stabiliser is its proximity to the plasma boundary. To determine the minimum permissible distance between the plasma boundary and the stabiliser surface, an experiment was conducted using a movable limiter. The methodology of this experiment is illustrated in figure 8.

The gyroradii of hot ions with energies of approximately 25 keV are comparable to the characteristic plasma radius. Consequently, the orbits of a significant fraction of hot ions extend beyond the plasma boundary.

In this experiment, the dependencies of the diamagnetic signal and fusion reaction rate on the radial position of the movable limiter were measured. These dependencies are presented in figure 9. The diamagnetic signal is proportional to the total energy content of the hot ion population, while the fusion reaction rate depends strongly on both the total number and the energy spectrum of hot ions.

https://doi.org/10.1017/S0022377826101913 Published online by Cambridge University Press

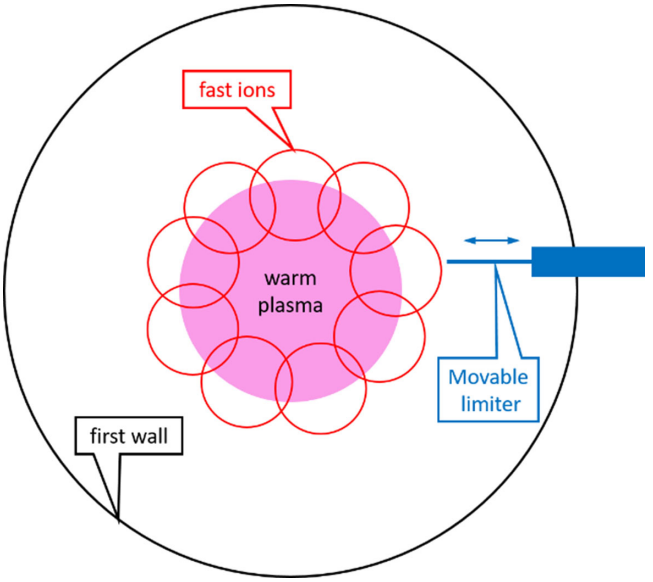


FIGURE 8. Method for determining the minimum permissible radius of the inner surface of a conducting stabiliser.

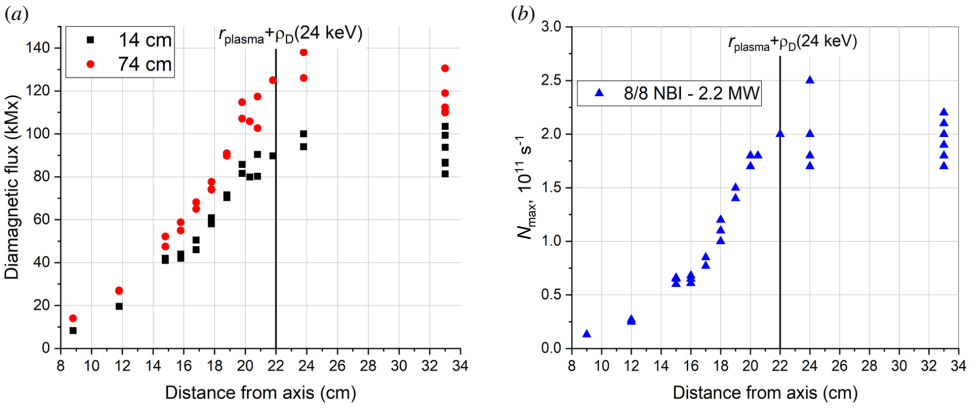


FIGURE 9. (*a*) Diamagnetic signals from loops positioned 14 and 74 cm from the central plane as a function of limiter radial position; (*b*) fusion reaction rate versus limiter position.

The data in figure 9 indicate that the inner radius of the conducting stabiliser may be set to 22 cm relative to the $r = 0$ axis. Based on these results and the analysis of Kotelnikov (2025), a preliminary design of the conducting stabiliser was developed. Its 3-D model is shown in figure 10.

As noted previously, successful demonstration of MHD stabilisation using a conducting wall at the GDT requires achieving $\beta \geqslant 0.8$ (Kotelnikov 2025). The maximum β value attained with the current GDT configuration is $\beta \approx 0.6$ (Simonen *et al.* 2010). To reach $\beta \geqslant 0.8$, two measures are planned:

https://doi.org/10.1017/S0022377826101913 Published online by Cambridge University Press

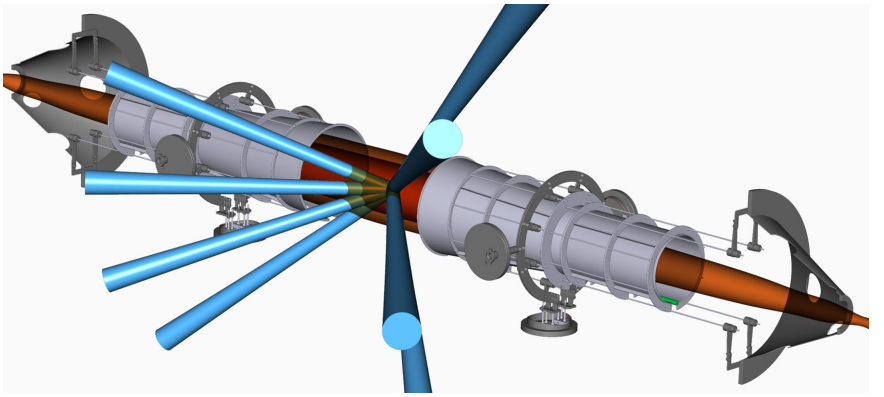


FIGURE 10. 3-D model of a conducting wall with an optimised configuration surrounding the plasma.

(i) extension of the neutral beam injection pulse duration from 5 ms to 10 ms to enhance plasma diamagnetism;
(ii) use of the recently upgraded electron cyclotron resonance heating system to increase the electron temperature $\langle T_e \rangle$, extend the confinement time of hot ions, and thereby boost both plasma diamagnetism and the volume-averaged beta $\langle \beta \rangle$.

6. New second-harmonic X-mode ECRH system at GDT

A new electron cyclotron resonance heating system for the GDT facility was developed during 2024–2025 (Khusainov *et al.* 2024). The system operates at the second harmonic of the X-mode with a frequency of 54.5 GHz, delivering up to 0.8 MW of microwave power for pulse durations of up to 10 ms. Figure 11 shows the layout of the upgraded ECRH system installed at GDT.

Preliminary experiments, the results of which are presented in figure 12, employed microwave injection from the low-field side (LFS), as illustrated in figure 11. During these experiments, the microwave power reaching the plasma boundary was 700 kW.

Although the preliminary results demonstrate a measurable increase in electron temperature, quasi-optical simulations (Khusainov *et al.* 2024) predict low absorption efficiency for LFS injection. Figure 13 compares the simulated power deposition for LFS and high-field side (HFS) injection scenarios. Only 45 % of the incident power is absorbed in LFS injection due to reflection from the resonance layer, whereas HFS injection eliminates this reflection and achieves 96 % absorption efficiency. Based on the experimental results and simulation predictions, HFS microwave injection is being implemented to achieve higher electron temperature.

Figure 14 shows the design of the HFS microwave launch system.

7. Plasma injection for bulk plasma particle balance using a Marshall gun

To address the challenge of maintaining particle balance in the bulk plasma, we investigated plasma injection using a Marshall gun (Rashleigh & Marshall 1978). Figure 15 illustrates the operating principle of the device.

https://doi.org/10.1017/S0022377826101913 Published online by Cambridge University Press

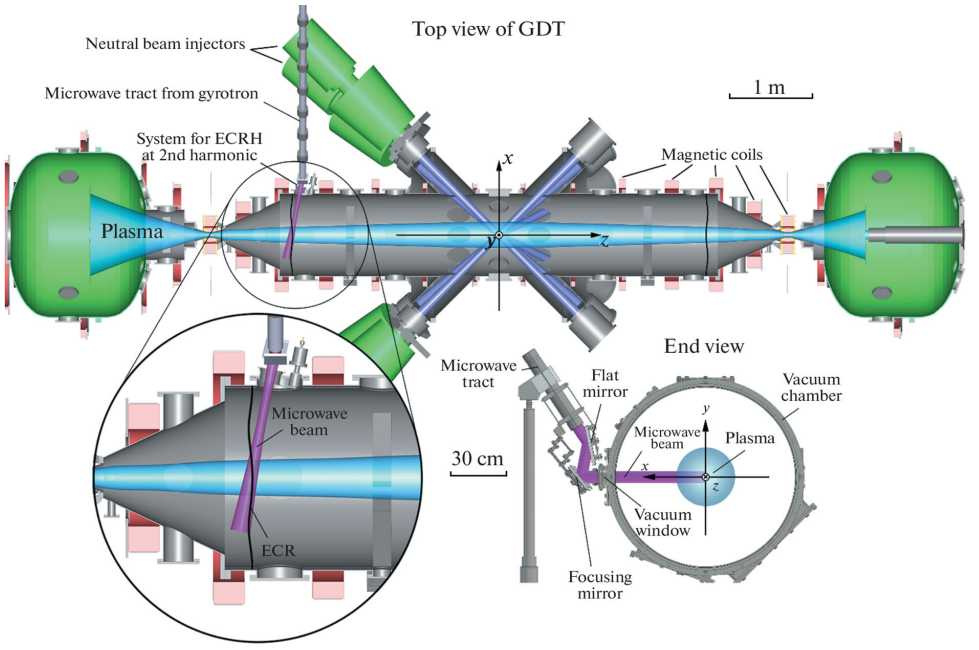


FIGURE 11. Layout of the upgraded second-harmonic X-mode ECRH system at GDT.

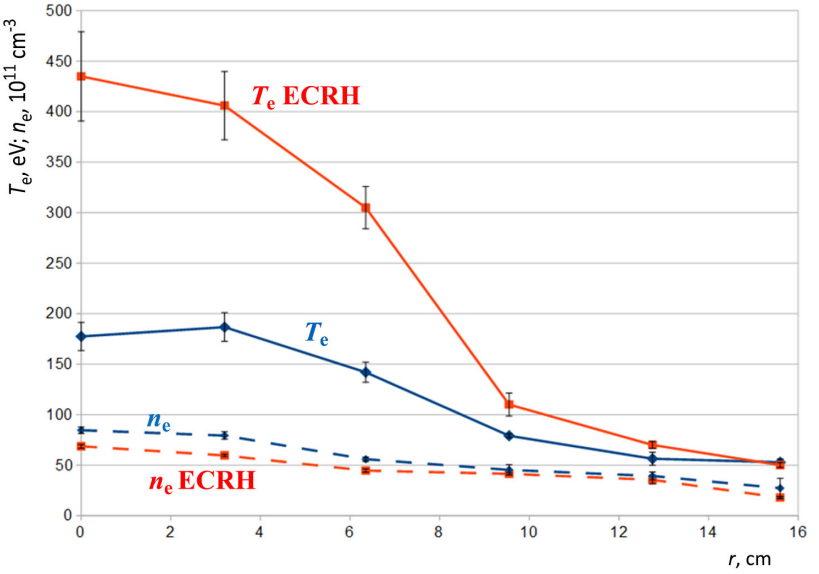


FIGURE 12. Radial profiles of electron density and temperature in discharges without ECRH (blue) and with ECRH applied (red) measured by Thomson scattering system and averaged over a series of discharges.

First, the gap between two coaxial electrodes is filled with hydrogen or deuterium gas. Application of a bias voltage creates an electric field (red arrows), triggering electrical breakdown in the gas. Then, the discharge current (yellow arrows) flows through the plasma and returns via the central electrode, generating an azimuthal

https://doi.org/10.1017/S0022377826101913 Published online by Cambridge University Press

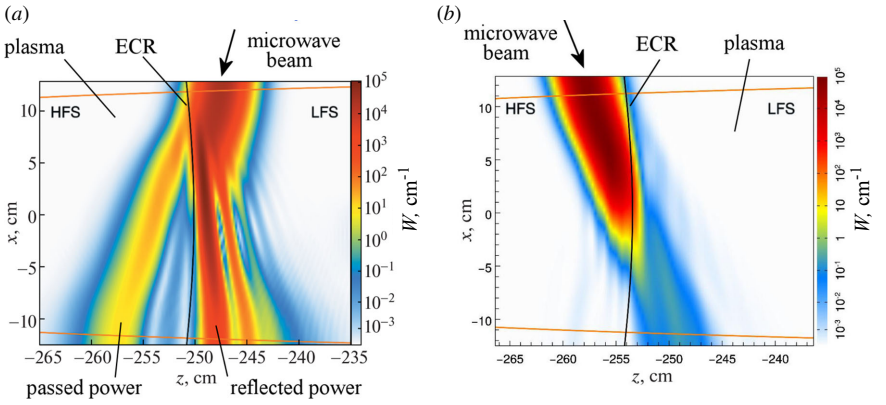


FIGURE 13. Quasi-optical simulation results for microwave injection from the (*a*) low-field side (LFS) and (*b*) high-field side (HFS) (Khusainov *et al.* 2024).

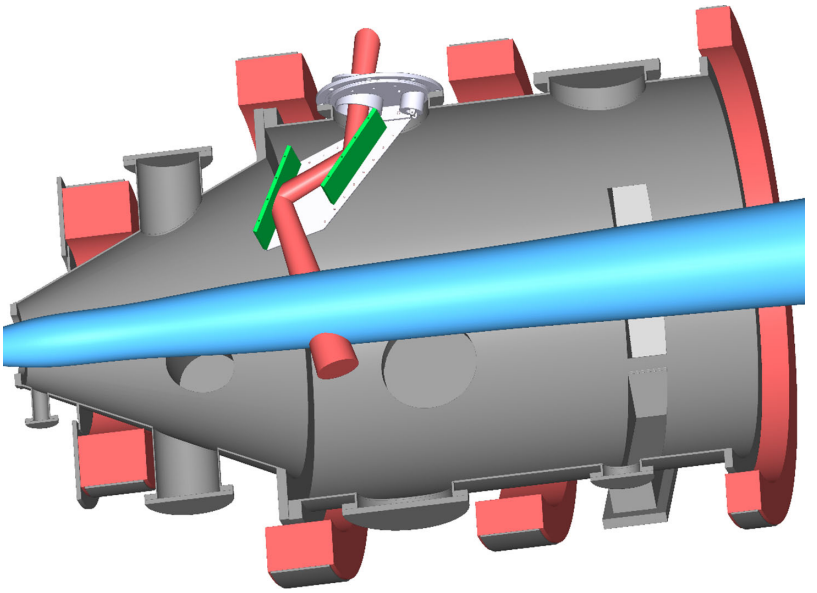


FIGURE 14. Design of the high-field side microwave launch system.

magnetic field (white arrows). The interaction between the radial current component in the plasma and the azimuthal magnetic field produces a Lorentz force that accelerates the plasma along the gun axis (blue arrows).

The parameters of the Marshall gun developed for GDT experiments are summarised in table 3.

The Marshall gun was installed in one of the GDT expander sections, replacing the standard arc plasma source (see figure 16). Results of preliminary injection experiments are presented in figure 17.

Based on these preliminary results, the Marshall gun can be considered a viable particle injector concept for the GDMT facility. Further development is required to create an injector based on this principle with near-unity gas utilisation efficiency

https://doi.org/10.1017/S0022377826101913 Published online by Cambridge University Press

Inner electrode diameter	1 cm
Outer electrode diameter	4 cm
Length of the device	100 cm
Accelerating current	10–100 kA
Pulse duration	50 μs
Capacity of power supply	600 μF
Voltage on the capacitor	2–5 kV

TABLE 3. Parameters of the Marshall gun developed for GDT experiments.

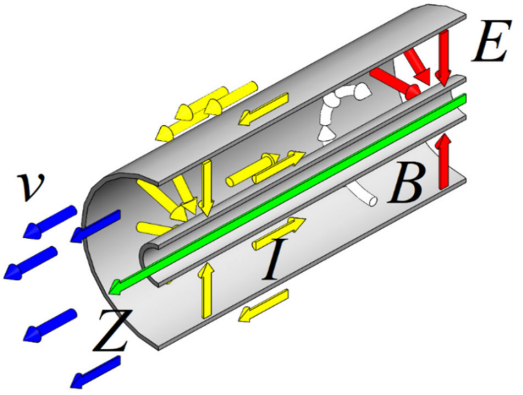


FIGURE 15. Operating principle of the Marshall gun.

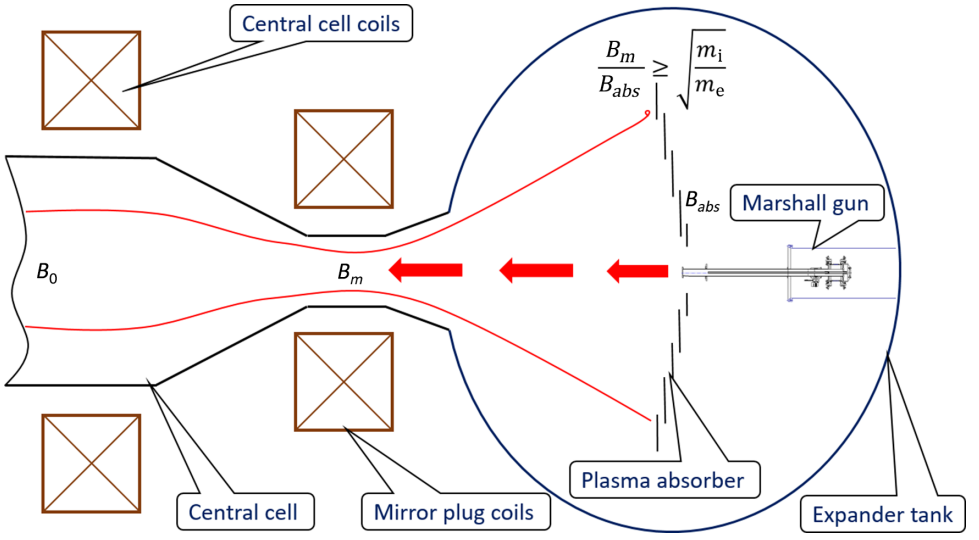


FIGURE 16. Installation of the Marshall gun in the expander section for plasma jet injection experiments.

https://doi.org/10.1017/S0022377826101913 Published online by Cambridge University Press

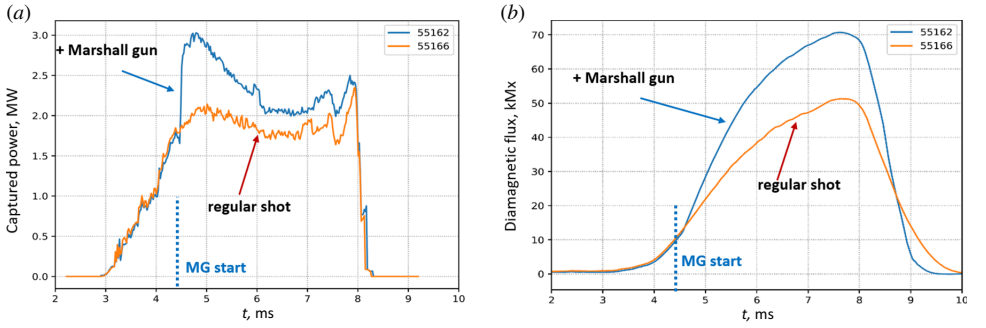


FIGURE 17. Results of preliminary Marshall gun injection experiments: (*a*) temporal evolution of neutral beam power captured by the plasma; (*b*) temporal evolution of the diamagnetic signal.

and a pulse repetition rate of ∼1 kHz, capable of delivering a cold particle flux equivalent to several kiloamperes of ion current into the axial region of the plasma column.

8. Conclusions

Experimental studies in support of the Gas-Dynamic Multiple-Mirror Trap (GDMT) concept are ongoing at the GDT facility. Key engineering systems and diagnostic suites have undergone substantial upgrades during the 2024–2025 campaign.

A preliminary design of an MHD stabilisation system based on a conducting wall has been developed, with an optimised inner radius of 22 cm determined experimentally.

A new second-harmonic X-mode ECRH system operating at 54.5 GHz has been commissioned. Preliminary experiments confirm the feasibility of this approach for electron heating, with quasi-optical simulations indicating that high-field-side injection will increase absorption efficiency from 45 % to 95 %.

The energy balance diagnostic system has been upgraded: an array of pyroelectric bolometers now spans the entire length of the GDT, enabling direct measurement of the total power flux from the plasma to the vacuum vessel wall.

Proof-of-principle experiments on bulk plasma fuelling using a Marshall gun injector have been successfully performed. The results support further development of this technique towards a high-repetition-rate (∼1 kHz) injector with near-unity gas utilisation efficiency for future GDMT-class devices.

Acknowledgements

Editor Cary Forest thanks the referees for their advice in evaluating this article.

Funding

The study was supported by the Ministry of Science and Higher Education of the Russian Federation.

Declaration of interests

The authors report no conflict of interest.

https://doi.org/10.1017/S0022377826101913 Published online by Cambridge University Press

REFERENCES

BAGRYANSKY, P.A., SHALASHOV, A.G., GOSPODCHIKOV, E.D., LIZUNOV, A.A., MAXIMOV, V.V., PRIKHODKO, V.V., SOLDATKINA, E.I., SOLOMAKHIN, A.L. & YAKOVLEV, DV. 2015 Threefold increase of the bulk electron temperature of plasma discharges in a magnetic mirror device. *Phys. Rev. Lett.* **114**, 205001.

BEKLEMISHEV, A.D. 2013 Helicoidal system for axial plasma pumping in linear traps. *Fusion Sci. Technol.* **63**, 355–357.

BEKLEMISHEV, A.D. 2016 Diamagnetic 'bubble' equilibria in linear traps. *Phys. Plasmas* **23**, 082506.

BEKLEMISHEV, A.D., BAGRYANSKY, P.A., CHASCHIN, M.S. & SOLDATKINA, E.I. 2010 Vortex confinement of plasmas in symmetric mirror traps. *Fusion Sci. Technol.* **57**, 351–360.

BERK, H.L., WONG, H.V. & TSANG, K.T. 1987 Theory of hot particle stability. *Phys. Fluids* **30**, 2681–2693.

BUDKER, G.I., MIRNOV, V.V. & RYUTOV, D.D. 1971 Influence of magnetic-field corrugation on expansion and cooling of a dense plasma. *JETP Lett.* **14**, 320–324.

IVANOV, A.A. & PRIKHODKO, V.V. 2013 Gas-dynamic trap: an overview of the concept and experimental results. *Plasma Phys. Control. Fusion* **55**, 063001.

KAISER, T.B. & PEARLSTEIN, L.D. 1985 Finite larmor radius and wall effects on the m = 1 ballooning mode at arbitrary beta in axisymmetric tandem mirrors. *Phys. Fluids* **28**, 1003–1005.

KHUSAINOV, T.A., BALAKIN, A.A., GOSPODCHIKOV, E.D., SOLOMAKHIN, A.L. & SHALASHOV, A.G. 2024 Quasi-optical simulations of scenarios with the second harmonic electron cyclotron plasma heating at the gdt facility. *Plasma Phys. Rep.* **50**, 1337–1352.

KOTELNIKOV, I.A. 2025 On the stability of the $m = 1$ rigid ballooning mode in a mirror trap with high-beta sloshing ions. *J. Plasma Phys.* **91**, E54.

LIZUNOV, A., BERBASSOVA, T., KHILCHENKO, A., MAXIMOV, V., PURYGA, E. & ZUBAREV, P. 2019 Integrated polychromator and data acquisition system for the Thomson scattering diagnostic. *J. Instrum.* **14**, C07010.

MOYZYKH, M. *et al.* 2026 Voyager fusion commercial power plant concept with open trap plasma confinement. *J. Plasma Phys.* in press.

PINZHENIN, E.I. & MAXIMOV, V.V. 2024 Application of nuclear physics methods for plasma diagnostics on a gas-dynamic trap. *Instrum. Exp. Tech.* **67**, 240–252.

POSTUPAEV, V.V. *et al.* 2017 The GOL-NB program: further steps in multiple-mirror confinement research. *Nucl. Fusion* **57**, 036012.

RASHLEIGH, S.C. & MARSHALL, R.A. 1978 Electromagnetic acceleration of macroparticles to high velocities. *J. Appl. Phys.* **49**, 2540–2542.

SIMONEN, T.C., ANIKEEV, A., BAGRYANSKY, P., BEKLEMISHEV, A., IVANOV, A., LIZUNOV, A., MAXIMOV, V., PRIKHODKO, V. & TSIDULKO, Y. 2010 High beta experiments in the GDT axisymmetric magnetic mirror. *J. Fusion Energy* **29**, 558–560.

SKOVORODIN, D.I. *et al.* 2023 Gas-dynamic multiple-mirror trap GDMT. *Plasma Phys. Rep.* **49**, 1039–1086.

SOLDATKINA, E.I. *et al.* 2025 The diagnostic complex and experiment control system at the GDT facility. *Plasma Phys. Rep.* **51**, 999–1051.

SOLDATKINA, E.I., MAXIMOV, V.V., PRIKHODKO, V.V., SAVKIN, V.Y., SKOVORODIN, D.I., YAKOVLEV, D.V. & BAGRYANSKY, PA. 2020 Measurements of axial energy loss from magnetic mirror trap. *Nucl. Fusion* **60**, 086009.

SOLDATKINA, E.I., MEYSTER, A.K., YAKOVLEV, D.V. & BAGRYANSKY, P.A. 2024 Experimental issues of energy balance in open magnetic trap. *J. Plasma Phys.* **90**, 975900203.

SUDNIKOV, A.V., IVANOV, I.A., INZHEVATKINA, A.A., KOZHEVNIKOV, A.V., POSTUPAEV, V.V., TOLKACHEV, M.S. & USTYUZHANIN, V.O. 2024 Improved axial confinement in the open trap by the combination of helical and short mirrors. *J. Plasma Phys.* **90**, 905900405.

YUROV, D.V., PRIKHODKO, V.V. & TSIDULKO, Y.A. 2016 Nonstationary model of an axisymmetric mirror trap with nonequilibrium plasma. *Plasma Phys. Rep.* **42**, 210–225.

ZAYTSEV, K.V. *et al.* 2014 Kinetic instability observations in the gas dynamic trap. *Phys. Scripta* **161**, 014004.

ZENG, Q. & KOTELNIKOV, I. 2024 Influence of the shape of a conducting chamber on the stability of rigid ballooning modes in a mirror trap. *Plasma Phys. Control. Fusion* **66**, 075020.

https://doi.org/10.1017/S0022377826101913 Published online by Cambridge University Press